PCCP

PAPER

Cite this: *Phys. Chem. Chem. Phys.*, 2018, **20**, 9298

Surfactants as mesogenic agents in layer-by-layer assembled polyelectrolyte/surfactant multilayers: nanoarchitectured "soft" thin films displaying a tailored mesostructure†

Esteban Piccinini,[a] Jimena S. Tuninetti,[a] Joseba Irigoyen Otamendi,[b] Sergio E. Moya,[b] Marcelo Ceolín,[a] Fernando Battaglini[c] and Omar Azzaroni*[a]

Received 7th December 2017,
Accepted 15th March 2018

DOI: 10.1039/c7cp08203g

rsc.li/pccp

Interfacial supramolecular architectures displaying mesoscale organized components are of fundamental importance for developing materials with novel or optimized properties. Nevertheless, engineering the multilayer assembly of different building blocks onto a surface and exerting control over the internal mesostructure of the resulting film is still a challenging task in materials science. In the present work we demonstrate that the integration of surfactants (as mesogenic agents) into layer-by-layer (LbL) assembled polyelectrolyte multilayers offers a straightforward approach to control the internal film organization at the mesoscale level. The mesostructure of films constituted of hexadecyltrimethylammonium bromide, CTAB, and polyacrylic acid, PAA (of different molecular weights), was characterized as a function of the number of assembled layers. Structural characterization of the multilayered films by grazing-incidence small-angle X-ray scattering (GISAXS), showed the formation of mesostructured composite polyelectrolyte assemblies. Interestingly, the $(PAA/CTA)_n$ assemblies prepared with low PAA molecular weight presented different mesostructural regimes which were dependent on the number of assembled layers: a lamellar mesophase for the first bilayers, and a hexagonal circular mesophase for $n \geq 7$. This interesting observation was explained in terms of the strong interaction between the substrate and the first layers leading to a particular mesophase. As the film increases its thickness, the prevalence of this strong interaction decreases and the supramolecular architecture exhibits a "bulk" mesophase. Finally, we demonstrated that the molecular weight of the polyelectrolyte has a considerable impact on the meso-organization for the $(PAA/CTA)_n$ assemblies. We consider that these studies open a path to new rational methodologies to construct "nanoarchitectured" polyelectrolyte multilayers.

Introduction

The assembly of nanocomponents into thin films displaying mesoscale organization is of paramount importance to create materials with novel or optimized properties.[1–9] A prerequisite for the construction of such functional interfaces is the development of methods for integrating molecular components with a strict control over the architecture (*i.e.*, organization and alignment). Research efforts on this matter are often referred to as "nanoarchitectonics", a term popularized by Ariga and co-workers.[10,11] Among different nanoconstruction techniques, the layer-by-layer (LbL) assembly represents an attractive bottom-up approach because of its versatility, simplicity and ability to control the vertical composition and film thickness with nanometric, or even molecular, precision. This technique was first reported by Iler in 1966,[12] and then extensively studied by Decher and Hong in the early 90s.[13,14] Nowadays, LbL is a firmly established method for the alternating adsorption of molecules mediated by a wide variety of interactions: electrostatics,[15] molecular recognition[16] and hydrogen bonding among others.[17,18] The construction of films through electrostatic

[a] *Instituto de Investigaciones Fisicoquímicas Teóricas y Aplicadas (INIFTA) – Departamento de Química, Facultad de Ciencias Exactas, Universidad Nacional de La Plata – CONICET, Suc. 4, CC 16, La Plata, Argentina. E-mail: azzaroni@inifta.unlp.edu.ar; Web: http://softmatter.quimica.unlp.edu.ar*
[b] *Soft Matter Nanotechnology Group, CIC BiomaGUNE. Paseo Miramón 182, 20009 San Sebastián, Gipuzkoa, Spain*
[c] *INQUIMAE, Departamento de Química Inorgánica, Analítica y Química Física, Facultad de Ciencias Exactas y Naturales, Universidad de Buenos Aires, Ciudad Universitaria, Pabellón 2 C1428EHA, Buenos Aires, Argentina*

† Electronic supplementary information (ESI) available: Additional GISAXS characterization. See DOI: 10.1039/c7cp08203g

interactions is particularly interesting because a large number of components of different nature are suitable as building blocks.[19–21] The concept of this approach relies on the alternating assembling of oppositely charged building blocks, positive and negative, onto charged interfaces.

Although the LbL technique offers excellent possibilities for creating nanocomposite thin films, the main research efforts with LbL have been focused on the construction of assemblies made of polycations and polyanions.[19] It has been reported that the internal structure of a series of $(A/B)_n$ polyelectrolyte films presented low degree of orientation and alignment of the constituents along the film.[15,22–24] Polyelectrolytes of each assembled layer significantly interpenetrate into neighbouring layers. Therefore, these films did not show Bragg peaks by X-ray reflectometry (XRR) or neutron reflectometry (NR).[25,26] However, a number of applications require the construction of interfacial nanoarchitectures addressing active functional groups in precise locations and orientations.[5,6,27] Therefore, the lack of true meso-scale organization in LbL films may be a limitation of this technique.

The interpenetration of polyelectrolytes in multilayer assemblies can be reduced by using mesogenic building blocks. Arys and co-workers reported that ordered multilayer films were obtained if polycations of the ionene family and specific polyanions were assembled.[25,28] Although these systems showed interesting nanoarchitectonic features, ionene polycations are not commercially available which may be an inconvenient from the viewpoint of practical, large-scale applications. To overcome this problem, the use of amphiphilic molecules – such as lipids and surfactants – as mesogenic agents could be a straightforward alternative to promote mesoorganization into these thin films.[11] These molecules, above certain concentration, have the property to self-assemble in water to form well organized entities (*e.g.* micelles, liquid-crystalline phases, *etc.*). Moreover, in combination with macromolecules they can lead to hierarchically organized hybrid materials with organization at the meso- and micrometric scale.[29,30] In fact, nature exploits the mesogenic properties of lipid amphiphilic molecules not only for the formation of lipid cell membranes, but also for the construction of organized assemblies made of lipids and cells such as the stratum corneum, the outermost layer of skin. In the stratum corneum, the lipids are arranged in a lamellar phase which confers to the skin the property to act as the main barrier for the diffusion of substances.[31] On the other hand, synthetic techniques that use the mesogenic property of surfactants for the construction of highly ordered mesostructured materials such as inorganic mesoporous,[32,33] and surfactant–polymer salt-complexes prepared by casting from organic solvents are well established.[34–36]

During the last two decades a number of works demonstrated that the integration of surfactants in the construction of surfactant–polyelectrolyte LbL films can lead to functional materials with marked surface, optical, and electronic properties.[37–42] Nevertheless, few works have studied the mesostructural properties of this sort of materials. Recently, Cortez *et al.* reported that the integration anionic surfactants, sodium dodecyl sulfate (SDS) and sodium octadecyl sulfate (ODS), in LbL assemblies of glucose oxidase (GOx) and osmium complex-modified poly(allylamine), *i.e.* $(OsPA/SDS/OsPA/GOx)_n$ or $(OsPA/ODS/OsPA/GOx)_n$, introduced mesostructural order in the supramolecular system.[5] The authors demonstrated that changes in the meso-organization significantly impacted on the bioelectrocatalytic features of these assemblies. However, it is still not clear how the internal mesoorganization of these supramolecular architectures evolves during the multilayer growth. In this work, we describe the formation of highly meso-organized $(A/B)_n$ thin films through the LbL assembly of polyacrylic acid (PAA) and hexadecyltrimethylammonium bromide (CTAB). First, the quartz crystal microbalance (QCM) technique was used to monitor the film growth and estimate the mass surface coverage. The PAA/CTAB chemical composition was studied by X-ray photoelectron spectroscopy (XPS) and the ionization degree of the PAA confined in the film was estimated by attenuated total reflectance (ATR) FTIR. Then, the internal organization of the components and its orientation with respect to the substrate was studied by grazing-incidence small angle X-ray scattering (GISAXS). By correlating GISAXS and QCM results, the mesostructure of the supramolecular architecture was obtained as a function of the film growth. Our results reveal that the strong interaction between the substrate and the first deposited layers yields a particular mesophase. As the film becomes thicker, this strong interaction becomes less preponderant and a "bulk" mesostructure prevails. In addition the $(PAA/CTA)_n$ multilayer assemblies were prepared using PAA of low (5 kDa) and high (450 kDa) molecular weight and the impact of the molecular weight of the polyelectrolyte on the film meso-organization was analyzed.

Materials and methods

2-Aminoethanothiol hydrochloride, (3-aminopropyl)-triethoxysilane (APTES), polyacrylic acid M_w 450 kDa (PAA_{450kDa}) and hexadecyltrimethylammonium bromide (CTAB) were purchased from Sigma-Aldrich. Polyacrylic acid M_w 5 kDa (PAA_{5kDa}) 50 wt% solution was purchased from ACROS Organics. All the polyelectrolyte and surfactant solutions were prepared with deionized water (resistivity around 18.2 MΩ cm^{-1}): 1 mg ml^{-1} PAA_{5kDa} (pH 3.7), 1 mg ml^{-1} PAA_{450kDa} (pH 3.7), 2 mM CTAB. As the PAA pK_a is between 5.5 and 6.5,[43] at pH 3.7 the PAA is mainly protonated (around 90%).[40] 1 mg ml^{-1} PAA solutions prepared with deionized water resulted in pH 3.7. This condition was chosen as a case study to be studied since it was reported that changes of pH and ionic strength can have important effects on the adsorbed polyelectrolyte mass.[43] The CTAB solutions were prepared over the critical micelle concentration (0.98 mM) at 25 °C in the absence of salt.[44]

Polyelectrolyte–surfactant LbL assembly

Cysteamine-modified gold surfaces were prepared as previously reported.[16] APTES-modified silicon wafers were prepared by vapor modification in a hermetic chamber during 24 hours at 20 °C. Both amino groups present in cysteamine and APTES confer a positive charge to the surface, that is crucial for the electrostatic self-assembly of the building blocks. APTES and cysteamine were carefully chosen since both compounds have

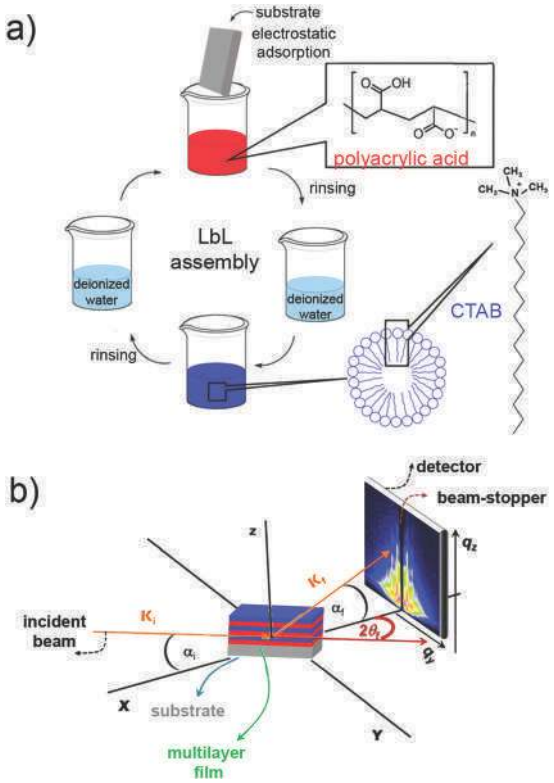

Scheme 1 (a) Representation of the PAA/CTAB layer-by-layer assembly. (b) Schematic of the experimental setup for the grazing-incidence small angle X-ray scattering measurements.

the same terminal group (primary amines), similar carbon chain length and they form stable self-assembled monolayers. As both surfaces (APTES-modified silicon wafer and cysteamine-modified gold) are exposing the same terminal groups the influence from the substrate is minimized. Layer-by-layer assemblies made of CTAB and PAA were prepared on the amine-terminated substrates (see Scheme 1a). PAA of low (5 kDa) and high (450 kDa) molecular weight were used. Each adsorption step was achieved by incubating the substrate in the polyanion or surfactant solution for 15 minutes followed by rinsing with deionized water for 2 minutes. The deposition cycle (n) is defined as the full cycle including incubation in the polyelectrolyte, the rinse in deionized water and the subsequent incubation in the surfactant solution followed by a water rinse.

Fourier transform infrared spectroscopy (FTIR)

Fourier transform infrared spectroscopy in the attenuated total reflection mode was performed using a Varian 600 FTIR spectrometer equipped with a ZnSe ATR crystal from PIKE technologies with a depth of penetration of the evanescent wave of 2 μm. The spectra were taken using a resolution of 1 cm^{-1}. Background-subtracted spectra were corrected for ATR acquisition. Two distinct absorption bands of the carboxylic acid functional groups were considered: the asymmetric stretching band of COO^-, ν = 1565–1542 cm^{-1}, and the C=O stretching of COOH, ν = 1710–1700 cm^{-1}. By assuming that the extinction coefficients for both bands are the same, the degree of ionization of PAA (α) at a given pH was calculated from: $\alpha = [\nu(COO^-)]/[\nu(COOH) + \nu(COO^-)] \times 100$ (%).[43] For FTIR measurements, the LbL films were prepared on cysteamine-modified gold substrates.

X-ray photoelectron spectroscopy (XPS)

An SPECS SAGE HR 100 system spectrometer was used. A Mg Kα (1253.6 eV) X-ray source was employed operating at 12.5 kV and 10 mA. The take-off angle was 90° and an operating pressure of 8×10^{-8} mbar was used. Quantitative analysis of spectra was carried out by using the Casa XPS software, employing Shirley baselines and Gaussian\Lorentzian functions. Surface-charging effects were corrected by setting the binding energy of the main component of the core level C1s at 284.6 eV.[45] For the determination of the O/N (oxygen/nitrogen ratio) ratio, calculations were performed by recording the XPS spectrum of ammonium bicarbonate powder in the same conditions as internal reference. To measure XPS, the multilayer assemblies were prepared on cysteamine-modified gold substrates.

Quartz crystal microbalance (QCM)

QCM measurements were carried out using the quartz crystal microbalance QCM200 from Stanford Research Systems and 5 MHz, AT-cut, 1 inch diameter gold-modified quartz crystals. The crystals were cleaned by immersing into a 1 : 1 : 5 solution of H_2O_2 (30%), ammonia (25%) and deionized water heated to a temperature of about 75 °C for 5 minutes. To study the film growth of the polyelectrolyte/surfactant multilayer assemblies, the frequency was measured after the adsorption of each component (CTAB or PAA) on cysteamine-modified gold QCM sensors. The frequency (f) was measured after dry the films with N_2. The mass surface coverage (Γ) was estimated by comparing the frequency before and after the assembly (Δf). Since f was measured in dried conditions and Δf was smaller than 2% of the bare crystal frequency (f_0), the Sauerbrey's equation is valid to be used:[46,47]

$$\Gamma = -\Delta f \times C_f \quad (1)$$

where C_f is the sensitivity factor with a value of 17.66 ng cm^{-2} Hz.

Atomic force microscopy (AFM)

A Veeco Multimode AFM connected to a Nanoscope V controller was used to image the multilayer films. AFM measurements were performed in tapping mode with maximum z-scale of 300 nm and a sample scan size of 6.5 μm × 6.5 μm. Non-conductive sharpened silicon nitride probe (Bruker, K = 0.12 N m^{-1}) were used.

Grazing-incidence small angle X-ray scattering (GISAXS)

GISAXS measurements were performed at the XRD2 beam-line of Laboratório Nacional de Luz Sincrotron (LNLS, Campinas, Brazil). A monochromatic beam of 8 keV (λ = 1.5497 Å) was used to perform the experiments. The slits were adjusted to obtain a beam width of 2 mm and height of 0.1 mm. GISAXS scattering intensities were recorded using a Pilatus 300k (DECTRIS Ltd) detector at a distance of 601 mm from the sample and with a pixel size of 0.172 mm × 0.172 mm. The exposure time to collect each scattering profile was 60 seconds. GISAXS experiments

were performed under ambient conditions: RH = 54% and T = 23 °C. The polyelectrolyte–surfactant multilayer assemblies were prepared on APTES-modified Si(100) wafers. The measurements were done with an incidence angle smaller than the Si total reflection angle previously obtained from X-ray reflectivity (XRR) experiments (see Scheme 1b). In order to maximize the information coming from the internal film structure, an incident angle of $\alpha_i = 0.20^\circ$ was chosen, which was between the critical angle for total reflection for the polymer, $\alpha_{c,P} = 0.1^\circ$, and the critical angle of the Si substrate, $\alpha_{c,Si} = 0.22^\circ$.

Surfactant–polymer films with lamellar mesostructures perpendicular to the substrate plane depict GISAXS patterns with diffraction fringes parallel to the q_z axis and at $q_{x,y}$ values at integer multiples of $2\pi/D_{lam}$. Being D_{lam} the lamellar thickness (*i.e.*, interplanar spacing). In this case, D_{lam} can be deduced from the $q_{x,y}$ position of the constructive interference as $D_{lam} = 2\pi/q_{x,y}$. For lamellar mesostructures aligned parallel to the substrate surface, the GISAXS patterns display a diffraction pattern along q_z following eqn (2):[48]

$$q_z = \frac{2\pi}{\lambda}\left(\sin(\alpha_i) + \sqrt{\sin^2(\alpha_{c,P}) + \left[\frac{m\lambda}{D_{lam}} \pm \sqrt{\sin^2(\alpha_i) - \sin^2(\alpha_{c,P})}\right]^2}\right) \quad (2)$$

where D_{lam} is the interplanar spacing, λ is the wavelength of the beam, α_i is the incidence angle of the X-ray beam with respect to the film surface. $\alpha_{c,P}$ is the critical angle of total external reflection of the polymer film and m is the order of the reflection. In case of symmetric lamellae m takes only odd values. The two branches of this curve correspond to the Bragg diffraction of the reflected beam (upper branch) and the direct diffraction process, which merges with the process where the diffracted beam is reflected from the substrate (lower branch). For each value of m, two peaks denoted the "minus branch" (M) and the "plus branch" (P) are expected in the GISAXS pattern.

On the other hand, randomly oriented lamellae present GISAXS patterns with rings around the reflected beam arising from multiple lamellar orientations relative to the substrate surface. The intensity of the ring is not homogeneously distributed along their circular shape because of the grazing incidence geometry. It has a maximum near the Yoneda peaks appearing at the q_z values corresponding to $\alpha_{c,P}$ and $\alpha_{c,Si}$, and decays toward high q_z.[48] Data analysis was done using FITGISAXS software.[49] GISAXS dispersion patterns were cut along the q_y axis at $q_z = 0.21$ nm^{-1} and $\Delta q_z = 0.13$ nm^{-1}, and along the q_z axis at $q_y = 0.16$ nm^{-1} and with a $\Delta q_y = 0.13$ nm^{-1}. To obtain the interplanar spacing D_{lam}, the scattering along q_z (out-of-plane) was analyzed by fitting the intensity profiles to a Gaussian function so that the peak position (q_p) and FWHM were quantitatively determined.

Results and discussion

Film thickness

The PAA and CTAB layer-by-layer adsorption on cysteamine-modified gold surfaces was monitored by QCM. Fig. 1 shows the frequency shifts, Δf, after the adsorption of each component for the assembly of 18 layers using PAA of low (5 kDa) and high (450 kDa) molecular weight (MW). The surface mass coverage, Γ, (Fig. 1 right axis) was estimated from Δf by using the eqn (1). Both systems displayed an exponential film growth and a similar Γ after the adsorption of 18th layers, *i.e.*: 9th deposition cycles (n). In this regard, additional microgravimetric studies comparing "dry" and "wet" films also revealed that the nominal mass of water confined in the films (m_{water}) increases upon adding layers to the assembly (see Fig. S4 in the ESI†).[50] However, since films exhibit an exponential increase in "PAA + CTAB" mass (m_{film}) during the LbL assembly, the water content, *i.e.*: $m_{water}/(m_{film} + m_{water})$ actually decreases during the subsequent deposition cycles (see Table S1 in the ESI†). Our systems display the typical supralinear growth behaviour exhibited by different multilayers assemblies. In this regard, Winnik and coworkers[51] already reported that this type of multilayers exhibit similar masses/coverages for low n, regardless of the molecular weight of the polyelectrolyte. The molecular mechanism behind the exponential growth of our multilayers is not clear; however, we observed that the growth pattern is highly reproducible. The molecular origin of this growth pattern will be investigated in a follow-up study.

Chemical composition

X-ray photoelectron spectroscopy (XPS) characterization was carried out in order to determine the chemical composition of the polyelectrolyte/surfactant multilayer assemblies. Fig. 2 shows the XPS core regions of O1s, N1s and C1s which were measured at high resolution. After spectra calibration (using the aliphatic C1s as reference) and baseline correction, the XPS signals can be quantitatively analyzed. From the atomic relative composition between O and N, the relation of PAA monomers units ($PAA_{monomer}$) and surfactant molecules can be obtained. The $PAA_{monomer}$/surfactant ratios were 2.1 and 2.0 for low and high PAA molecular weight respectively. By the deconvolution of the C1s core region spectra (Fig. 2), the carboxylic (COOH, 288.6 eV) and carboxylate (COO^-, 287.4 eV) components, from

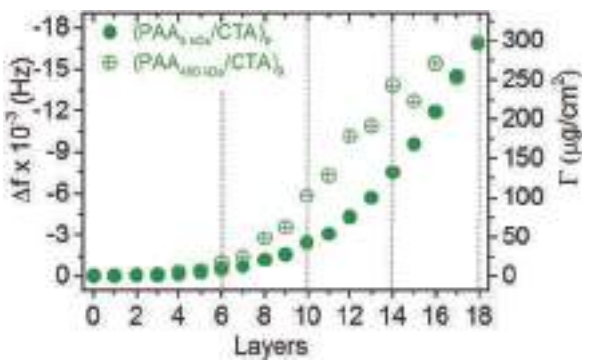

Fig. 1 Change of frequency (Δf) obtained by QCM as a function of the number of layers for $(PAA_{5kDa}/CTA)_n$ (solid circles) and $(PAA_{450kDa}/CTA)_n$ (open circles) multilayer assemblies. The frequency was measured at air atmosphere after each adsorption step. The mass surface coverage (Γ) was estimated by using the Sauerbrey's equation.

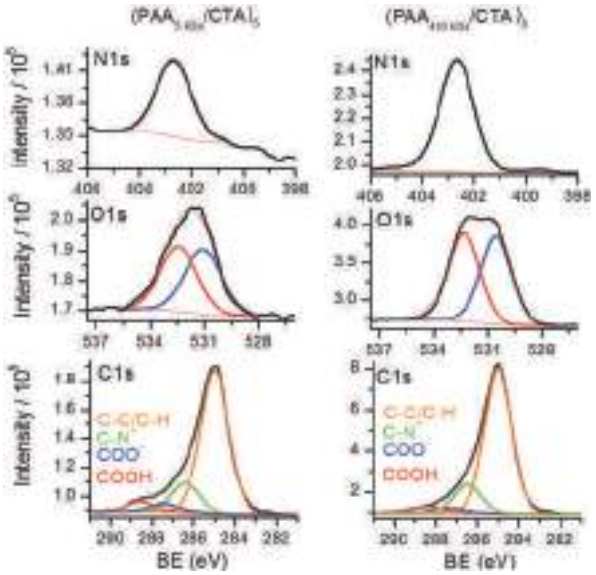

Fig. 2 X-ray photoelectron spectroscopy (XPS) O1s, N1s and C1s spectra of $(PAA/CTA)_5$ films prepared with low (5 kDa) and high PAA molecular weight (450 kDa). The LbL assemblies were prepared on cysteamine-modified Au substrates.

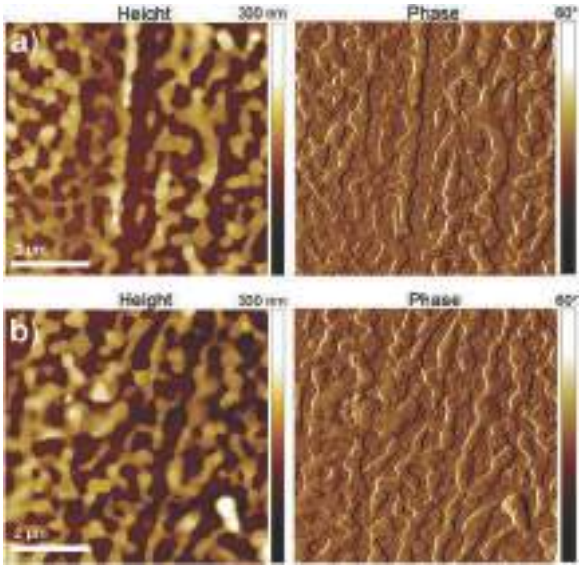

Fig. 3 AFM image corresponding to topographic (left) and phase (right) imaging of (a) $(PAA_{5kDa}/CTA)_5$ and (b) $(PAA_{450kDa}/CTA)_5$ multilayer assemblies (tapping mode; maximum z-scale: 300 nm; scan size: 6.5 μm × 6.5 μm).

the PAA, and the quaternary amine-carbon ($C–N^+$, 286.4 eV) component, from the CTAB, where resolved. Although the adventitious carbon complicates any accurate quantification, the presence of carboxylic and carboxylate groups reveals that PAA was not fully ionized.

It is important to point out that no detectable amount of Br^- counterion was present in the films. Therefore, the positive charge of the surfactant quaternary ammonium group was intrinsically compensated by the PAA carboxylic acid groups. This result is in agreement with the typical behaviour of polyanion/polycation multilayer films.[52] Furthermore, the absence of significant amount of counterions inside the film could be related to the formation of highly dense films.[53]

Surface morphology

Topographic and phase AFM images of the as-prepared PAA/CTA films on silicon wafers with 5 deposition cycles are depicted in Fig. 3. For both samples, islands formed on the substrate were visualized, thus evidencing that the surface topography is rather irregular. It can also be appreciated (mainly in the phase images) that the islands are randomly distributed and some of them are connected. We should note that the valleys in the topographic images do not correspond to bare substrate surface. The lack of contrast in the phase images are a clear indication that the "physicochemical nature" of the film is homogeneous across the surface. Hence, in principle, we can rule out the presence of bare domains in the AFM image, even if the topographic images are inhomogeneous.[54] The variation of the molecular weight of PAA did not showed appreciable differences in the topographic features of the films. Regarding the origin of surface patterns observed on the samples, it was previously reported that it is possible to form spontaneously periodic horizontal striped assemblies on energetically uniform surfaces by vertical dip coating if the surface is withdrawn slowly from a colloidal solution.[55] Since our layer-by-layer assemblies were prepared by vertical dipping the substrate in the polyelectrolyte solutions and then in water (for the rinsing step), the slight alignment and the elongated shape of the polyelectrolyte–surfactant assemblies might be ascribed to phenomenon reported by Ghosh *et al.* Similar surface patterns have been also observed in LbL-grown PDADMAC/PSS multilayers[56] and cetyltrimethylammonium bromide (CTAB)/polyacrylic acid (PAA).[57]

Degree of ionization of PAA confined in the film

The ionization degree of the PAA confined in the film was estimated by attenuated total reflection Fourier-transform infrared (FTIR) spectroscopy.[43] Table 1 shows the degree of ionization of PAA in $(PAA/CTA)_n$ assemblies for n = 3, 5, 7 and 9. Trends were similar for both PAA molecular weights, showing that during the first deposition cycles the ionization degree was near 30% and the value slightly decreased with the number of deposited layers (see Fig. 4). The results showed an increase of the degree of ionization when the PAA is confined in the LbL assembly from 10% (PAA in solution pH 3.7) to 20–30%. This behaviour was expected since the apparent pK_a value of weak polyelectrolytes such as PAA decreases when the polymer

Table 1 Ionization degree (in percentage) of $(PAA/CTA)_n$ LbL assemblies prepared from low and high molecular weight

n	$(PAA_{5kDa}/CTA)_n$	$(PAA_{450kDa}/CTA)_n$
3	33	29
5	33	34
7	23	26
9	20	22

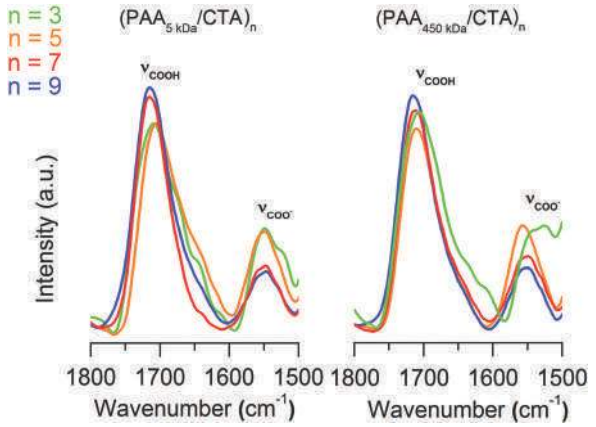

Fig. 4 Attenuated total reflection FTIR for $(PAA/CTA)_n$ multilayer assemblies (n = 3, 5, 7 and 9) prepared with low and high molecular weight.

chain is incorporated into a multilayer system due to electrostatic and hydrophobic interactions between the self-assembled components.[43]

Typical examples of addition of ionic surfactants to a solution of oppositely charged polyelectrolytes reveal the formation of polyelectrolyte–surfactant "salt-complexes" exhibiting a strict 1 : 1 stoichiometry.[58,59] Even though the formation of these complexes relied on the use of polyacrylate instead of polyacrylic acid, this behaviour was also reported for polyelectrolyte–surfactant complexes prepared from polyacrylic acid and quaternary ammonium surfactants.[36] On the contrary, our results evidence that the construction of polyelectrolyte–surfactant assemblies using the LbL technique differ from typical results obtained through bulk complexation. In addition, we should not that FTIR and XPS characterization does not provide the same quantitative assessment. We hypothesize that differences that arise between XPS and FTIR results stems from the sensitivities and analysis depths of both techniques. As is well known, FTIR sensitivity is not as good as XPS, and on the other hand, XPS exhibits a low analyzing depth ($\sim$5 nm) as compared to FTIR. However, XPS measurements are time-consuming. Compared to XPS, FTIR spectroscopy is a fast technique, but FTIR spectroscopy – in some cases – is believed to be of no use to characterize surface modifications at the top nanometer levels because predominately the bulk material is studied. In the case of ATR-FTIR, the penetration depth into the sample is typically between 0.5 and 2 microns. It is for these reasons that we consider that that FTIR provides more reliable statistical information about the multilayer composition across the film thickness.

Mesostructural characterization

Grazing-incidence X-ray scattering (GISAXS) was used to characterize the internal structure of the $(PAA/CTA)_n$ multilayer films. This technique offers an unique, non-invasive method to obtain information of both lateral and transverse structures inside thin films and their orientation with respect to the substrate surface.[60] Moreover, GISAXS is well suited for structural characterization of thin films because in the grazing-incidence configuration the X-ray beam path through the film is long enough to assure a high statistical significance, which translates into a high intensity scattering pattern.[61] In our studies, the internal organization of the films was characterized as a function of the number of deposition cycles. In general, the PAA/CTA multilayer assemblies showed high degree of internal meso-organization (Fig. 5 and 7) for n above 3. Both systems (low and high MW) showed intense diffraction constructive interferences, which evidence the presence of meso-organization highly correlated along the film.

In particular for the assemblies prepared with the polyelectrolyte of low MW, the meso-organization was significantly dependent on the number of deposition cycles (Fig. 5). For 3 deposition cycles (Fig. 5a), the GISAXS pattern shows a double diffraction spot on the q_z wavevector transfer coordinate (q_y = 0). This pattern is characteristic of lamellae parallel to the substrate surface,[48] where two spots are expected to appear at q_y = 0 being the "minus branch" (M) and the "plus branch" (P). The distance between the lamellae along the z direction of the film (D_{lam}) was calculated using eqn (2) and the obtained D_{lam} value was 3.97 nm, which is slightly higher than that reported for PSS-CTA salt complex films (3.52 nm).[58] Weak additional pair of spots at an angle of 33° can be seen in Fig. 5a, suggesting that the polymer–surfactant layers assembled not only following the predominant mesostructures described in the text but forming minority-structure domains possibly related to local strains or defects.

It can be seen in the GISAXS pattern of the $(PAA_{5kDa}/CTA)_5$ assembly (Fig. 5b) that an intense spot at q_y = 0 overlaps with a low intensity halo. The halo evidences the presence of multi-ordered lamellar domains.[62,63] Since the intensity of the halo is larger at q_y = 0, it can be suggested that the preferential orientation of the lamellae domains is parallel to the surface. PAA/CTA assemblies of 7 or 9 deposition cycles (Fig. 5c and d) showed, in addition to the 2D lamellar spot, an in-plane ($q_z \approx 0$) pair of spots and an out-of-plane pair of spots at q_z = 1.7 nm^{-1}. This pattern is characteristic of circular hexagonal mesostructures forming rings with their axis perpendicular to the substrate (see scheme in Fig. 6).[64–66] The theoretical X-ray dispersion pattern of this mesostructure was previously demonstrated by Marlow *et al.* who solved the ring structure in the reciprocal space.[64] Although this interesting mesostructure was reported for films confined in nanoporous membrane,[65,66] it is worth noting that this mesostructural feature has neither been observed in LbL assemblies nor even in planar thin films.

As can be seen for assemblies with n = 7 and 9, GISAXS patterns evidenced the coexistence of two different mesostructures. To obtain a qualitatively view of the predominant mesostructure during the construction of the multilayer assembly, intensities of the circular hexagonal and lamellar spots were compared as a function of the number of bilayers (blue circles in Fig. 6). This correlation indicates that there is a notable increase in the circular hexagonal intensity ($I_{cir\,hex}$) as compared to the lamellar intensity (I_{lam}) upon increasing the number of bilayers. Moreover, the full width at half maximum (FWHM) of the circular hexagonal spots (red circles) became narrower suggesting an increasing amount of the hexagonal domains.

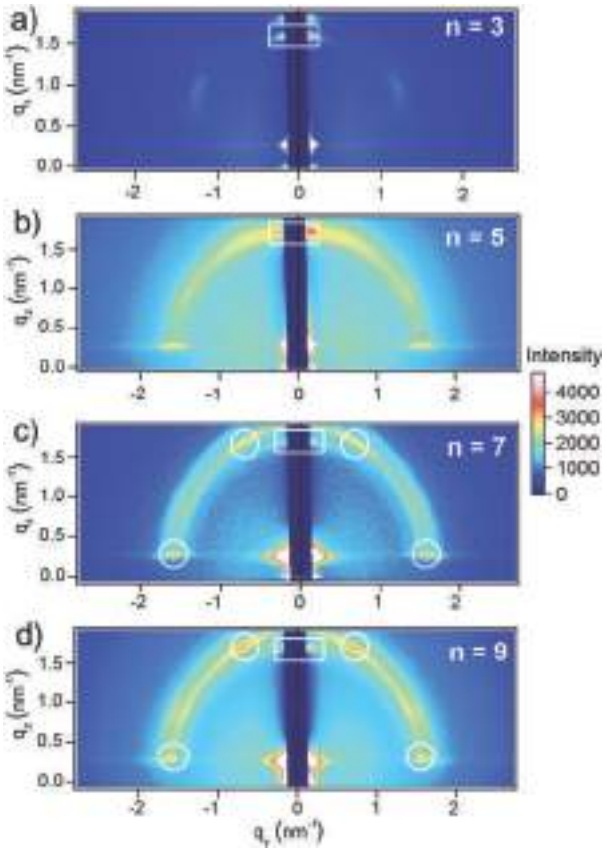

Fig. 5 GISAXS patterns obtained from $(PAA_{5kDa}/CTA)_n$ assemblies of different number of bilayers: 3 (a), 5 (b), 7 (c) and 9 (d). The films were prepared on APTES-modified Si(100) substrates and measured at an incident angle (α_i) of 0.2°. Squares show the diffraction pattern from a lamellar mesophase, while circles show the diffraction pattern from a circular hexagonal mesophase.

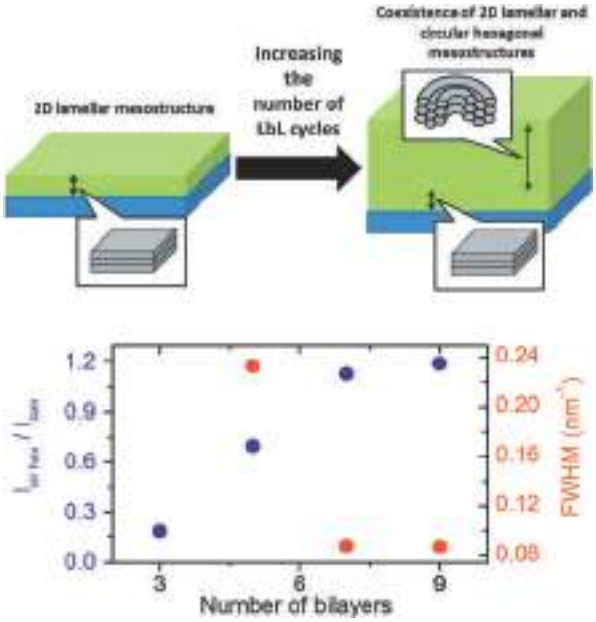

Fig. 6 Top: Schematic representation of the meso-organization for thin and thick multilayer assemblies. Bottom: Intensity ratio between the circular hexagonal ($I_{cir\,hex}$) and lamellae (I_{lam}) spots as a function of the number of bilayers (blue circles). At the right *y*-axis, full-width of half maximum (red spots) from the spots of the circular hexagonal mesostructure.

These results evidenced that the predominant mesostructure changed from lamellar (parallel to the surface) to circular hexagonal (with the axis perpendicular to the surface) as the film thickness increased.

Although a change of the predominant mesostructure was obtained for high values of n, the spot corresponding to the lamellar mesostructure did not completely vanish. Therefore, two different architectonic scenarios could be presented for $n \geq 7$: (a) both mesophases are present along the film (b) the lamellar mesophase is present in the first assembled layers, and the subsequent layers display a hexagonal mesophase. To elucidate the more plausible scenario, GISAXS experiments were performed with a smaller angle of incidence and, thus, collecting more structural information from the outermost layers. The maximum intensity of the lamellar diffraction fringes decreased by decreasing the incidence angle (Fig. S1, ESI†), evidencing that the outermost layer did not exhibit a lamellar mesophase. These results suggest that the films presented an internal organization as the scenario (b), which is illustrated in Fig. 6. A possible explanation for this phenomenon might be ascribed to the strong interfacial interactions among the first layers and the substrate inducing a lamellar organization. A rather similar effect was observed in different properties of thin polymeric films.[67,68] For example, it is well-known that thermal properties of thin films are themselves functions of film thickness and strongly influenced by interfacial interactions.[69,70] Interfacial confinement can promote spatial configurations that ultimately lead to a particular substrate-induced meso-organization.[71,72] On the other hand, as the film becomes thicker, the "stressed" layers are less predominant and the circular hexagonal mesostructure prevails.[73]

To obtain the periodic distance between the mesostructures, the GISAXS dispersion patterns were cut along the q_z axis (out-of-plane). Table 2 shows the position of the diffraction peaks (q_p) and the interplanar spacing (D_{lam}) obtained from the q_z-cuts (Fig. S2, ESI†) using eqn (2). Interestingly, the periodic distance decreased from 3.97 (n = 3) to 3.73 nm (n = 9) as the film thickness increased. The diminution of the mesostructural spacing is consistent with the decrease in the PAA ionization degree measured by FTIR. Since the film can be considered as electro-neutral and the counter ion concentration (*i.e.*, Br^-) is

Table 2 Values of out-of-plane q_p and periodic distance as well as the predominant mesophase for the $(PAA_{5kDa}/CTA)_n$ assemblies as a function of the number of bilayers. The error of the periodic spacing estimation is ±0.03 nm

n	Predominant mesostructure	q_p (nm^{-1})	Periodic spacing (nm)
3	Lamellar parallel to the surface	1.59	3.97
5	Lamellar (multioriented)	1.72	3.67
7	Lamellar/circular hexagonal	1.68	3.76
9	Lamellar/circular hexagonal	1.69	3.73

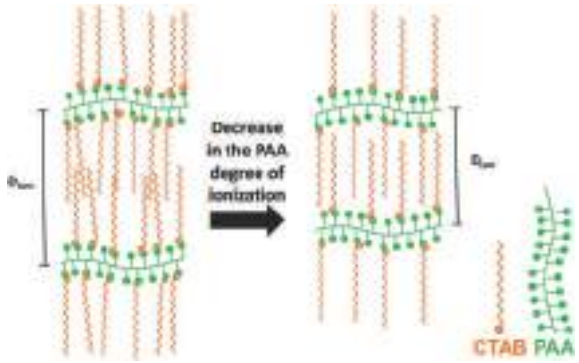

Scheme 2 Schematic picture that illustrates how the decrease in the degree of ionization of PAA impacts on the mesostructure of the multilayer assemblies.

negligible, the decrease in the PAA ionization degree implies that the $PAA_{monomer}$/CTA ratio should increase. As the aliphatic chains from the CTAB acts as mesostructural spacers, a decrease in the periodic distance is expected if the CTAB proportion in the film also decreases (see Scheme 2). Note. however, that an additional mass of uncharged PAA per surfactant molecule would increase the periodicity.

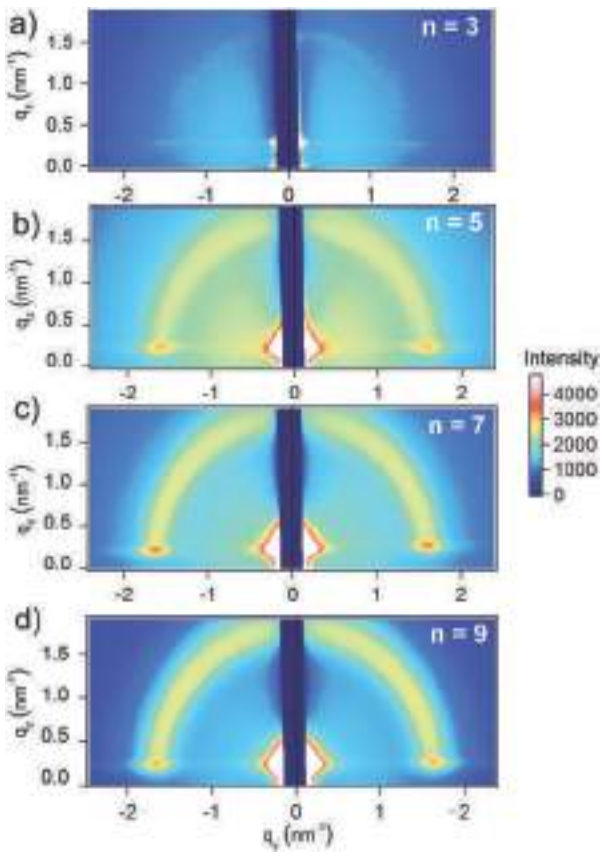

Fig. 7 GISAXS patterns obtained from $(PAA_{450kDa}/CTA)_n$ assemblies of different number of bilayers: 3 (a), 5 (b), 7 (c) and 9 (d). The films were prepared on APTES-modified Si(100) substrates and measured at an incident angle (α_i) of 0.2°.

Table 3 Values of out-of-plane q_p and periodic distance as well as the predominant mesophase for the $(PAA_{450kDa}/CTA)_n$ assemblies as a function of the number of bilayers. The error of the periodic spacing estimation is ±0.03 nm

n	Predominant mesostructure	q_p (nm^{-1})	Periodic spacing (nm)
3	Lamellar (multioriented)	1.58	3.99
5	Lamellar (multioriented)	1.70	3.72
7	Lamellar (multioriented)	1.78	3.55
9	Lamellar (multioriented)	1.8	3.51

The internal meso-organization of multilayered films prepared with PAA of high MW was also studied. The GISAXS dispersion patterns (Fig. 7) showed a well defined halo corresponding to randomly oriented lamellae. The periodic distance between lamellae was estimated by performing out-of-plane cuts of the GISAXS pattern (see Fig. S3, ESI† and Table 3). The periodic spacing between lamellae decreased from 3.99 to 3.51 nm by increasing the number of bilayers, in a similar fashion to the assemblies made of low MW PAA.

It is important to note that although the film prepared with low and high MW showed similar growth characteristics, PAA:CTA stoichiometry and surface morphology, the structural features were markedly different (see Fig. 5d and Fig. 7d). Therefore, we can infer that the molecular weight of the poyelectrolyte also plays an important role on the internal meso-organization. This behaviour is in agreement with those reported by Piculell and co-workers for PAA–CTAB ''salt complex'' in aqueous medium.[74] They reported a liquid crystal phase transition when the polyanion exceeded a value of 5 kDa. They argued that the dependence of the mesophase with the polyelectrolyte molecular weight is due to a translational entropy change by increasing the amount of monomer units per polymer chain.[75] In our case, our interpretation is based on the fact that, compared to low MW polymers, high MW polymers exhibit a higher number of ''sticking points'' (per macromolecule) connecting to the adjacent layers. As a result, the spatial reconfiguration of high MW polymers during the LbL assembly process is a costly process in comparison to low MW polymers. Or, in other words, low MW polymer are more easily reconfigured during the self-assembly process, thus facilitating access to different mesostructures.

Conclusions and remarks

A sophisticated reader, casting a glance at this paper, might say: can layer-by-layer assembly make a difference when it comes to the formation of polyelectrolyte–surfactant complexes on surfaces? Why don't we simply use solution casting of polyion–surfactant ion ''complex salts''?

Answering these questions implies comparing both techniques. However, a direct comparison between both systems without a proper discussion could be misleading and – to some extent – unfair. By way of conclusion, let us therefore compare these systems in detail and summarize some fundamental issues concerning the layer-by-layer formation of mesostructured assemblies.

(a) The formation of thin films through solution casting of polyion–surfactant ion ''complex salts'' relies on the generation of polyelectrolyte–surfactant complexes in bulk solution. Conversely, our approach is based on assembling polyelectrolytes and surfactants in a LbL fashion. In one case the complexation process takes place in solution whereas in the other case the complexation is taking place on the surface during the assembly process. In general, solution casting of polyion–surfactant ion ''complex salts'' proceeds in non-aqueous solvents, *e.g.*: ethanol. On the contrary, our self-assembly process takes place entirely in aqueous solutions. These factors lead to major differences between both approaches.

(b) It seems plausible to consider that these underlying differences translate into considerable structural variations in the film mesostructure. For example, Picculell and co-workers studied the structure of films generated *via* solution casting of ''complex salts'', composed of cationic alkyltrimethylammonium surfactants with polyacrylate counterions, on mica surfaces.[76] These authors observed that – depending on the experimental conditions – films exhibited different mesostructures, including cubic, hexagonal and rectangular structures, but no lamellar structures. We believe that the reason behind the absence of lamellar phases in these experiments is the absence of strong interfacial interactions. As aforementioned, these systems are created in bulk and then transferred to the solid substrate. In this regard, we must refer to seminal works by Russell and his collaborators on amphiphilic block copolymer assembly on surfaces. These authors demonstrated that interfacial interactions can induce lamellar orientation in a wide variety of charged amphiphilic macromolecular films.[77,78] In this sense, our experimental evidence hints that the strong interfacial interactions taking place during the layer-by-layer assembly process play a role in defining the mesostructure of the multilayered architecture.

(c) A detailed analysis of the literature reveals that there are increasing numbers of cases in which there is an erroneous assumption that a well-defined ''one-dimensional'' SAXS (or XRD) pattern reflects the 3D mesoscale organization of a particular material deposited on a given substrate. For instance, in some examples of films generated *via* solution casting of ''complex salts'' claiming 3D organization or even preferential orientation, the reported data are limited to 1D SAXS plots, or 2D-SAXS plots displaying bright halos instead of bright spots, thus evidencing that the mesoscopic domains are randomly oriented with respect to the substrate. One of the remarkable aspects of our approach is the use of LbL assembly and surfactants to tailor the 3D mesoscale organization of the assembled film. In other words, we demonstrate that the mesoscale domains display a specific orientation with respect to the substrate, as corroborated by grazing-incidence small-angle-X-ray scattering (GISAXS) characterization.

(d) By studying the internal meso-organization and the film growth, it was observed that the mesostructural characteristics (*i.e.*, mesophase and periodic spacing) vary as a function of the film thickness. In particular for $(PAA/CTA)_n$ assemblies prepared with a low molecular weight PAA, two mesostructural regimes were observed: a lamellar mesophase for the first deposition cycles ($n \leq 3$), whereas a coexistence of circular hexagonal and lamellar mesostructures prevails for $n \geq 7$. From these results, it is hypothesized that the strong interaction with the substrate, given its high surface charge density and flat geometry, likely contributes to the lamellar ordering of the first layers. As the film becomes thicker, the tension vanishes and the supramolecular architecture evolves to a circular hexagonal mesophase. Moreover, we have observed a decrease in the periodic spacing as a function of the film growth. This result was explained in terms of the change in the ionization degree of PAA. Finally, the use of a high molecular weight PAA resulted in $(PAA/CTA)_n$ assemblies with a multioriented lamellar mesophase. Therefore, the polyelectrolyte molecular weight has an important effect on the film internal organization.

(e) The use of surfactants in the LbL technique allows not only the formation of nanocomposite thin films integrating hydrophobic moieties but also offers a strategy to control the internal meso-organization of the multilayers. Unlike other techniques that also allow the construction of polyelectrolyte/surfactant mesostructured films,[34,36,79,80] the approach reported here presents the following advantages: (i) the film is directly prepared on a solid surface (ii) the film thickness is easily controlled with nanometric precision by the number of adsorbed layers (iii) well-defined film mesostructures displaying tailored spatial configurations can be obtained, a feature that is essential for a number of applications where a vectorial transfer of energy, electrons, or matter is required.

(f) While it is certainly true that materials science is getting more sophisticated, it is also true to say that sometimes we need to draw upon ''old'' concepts to face new challenges. In this sense, we demonstrated that the combination of two worlds, LbL assembly and polyelectrolyte–surfactant complexes, offers new horizons for creating ''soft'' interfacial assemblies displaying tailorable mesostructures. In fact, we consider that these results are relevant for the further development of ''thin film nanoarchitectonics'' provided that structural complexity induced by the presence mesoscale organized domains can define the functional properties of self-assembled multilayers.

Conflicts of interest

There are no conflicts to declare.

Acknowledgements

This work was supported by CONICET (PIP 0370), ANPCyT (PICT-2010-2554, PICT-2013-0905, PICT-2014-3377) and UNLP (PPID-X016). E. P. gratefully acknowledges CONICET for a doctoral scholarship. J. S. T., M. C., F. B. and O. A. are staff researchers of CONICET. O. A. and M. C. gratefully acknowledge the Laboratório Nacional de Luz Síncrotron (LNLS, Campinas-Brazil) for financial support and granting access to synchrotron facilities (XRD2-13391; XRD2-11639, XRD2-14358 and SXS-11642). E. P. thanks Andrés Piccinini for helpful discussions.

Notes and references

1 C. M. Palumbiny, F. Liu, T. P. Russell, A. Hexemer, C. Wang and P. Müller-Buschbaum, *Adv. Mater.*, 2015, **27**, 3391–3397.
2 J. Y. Park and R. C. Advincula, *Soft Matter*, 2011, **7**, 9829.
3 P. Liu, S. Dong, F. Liu, X. Hu, L. Liu, Y. Jin, S. Liu, X. Gong, T. P. Russell, F. Huang and Y. Cao, *Adv. Funct. Mater.*, 2015, **25**, 6458–6469.
4 D. T. Balogh, M. Ferreira and O. N. Oliveria, in *Functional Polymer Films*, ed. R. C. Advincula and W. Knoll, Wiley-VCH Verlag & Co. KGaA, Weinheim, Germany, 2011, pp. 113–149.
5 M. L. Cortez, N. De Matteis, M. Ceolín, W. Knoll, F. Battaglini and O. Azzaroni, *Phys. Chem. Chem. Phys.*, 2014, **16**, 20844–20855.
6 K. Ariga, Q. Ji, T. Mori, M. Naito, Y. Yamauchi, H. Abe and J. P. Hill, *Chem. Soc. Rev.*, 2013, **42**, 6322–6345.
7 K. Ariga, Y. Yamauchi, G. Rydzek, Q. Ji, Y. Yonamine, K. C.-W. Wu and J. P. Hill, *Chem. Soc. Jpn.*, 2014, **43**, 36–68.
8 K. Ariga, A. Vinu, Y. Yamauchi, Q. Ji and J. P. Hill, *Chem. Soc. Jpn.*, 2012, **85**, 1–32.
9 J. Wang, J. Tang, B. Ding, V. Malgras, Z. Chang, X. Hao, Y. Wang, H. Dou, X. Zhang and Y. Yamauchi, *Nat. Commun.*, 2017, **8**, 1–9.
10 M. Aono, Y. Bando and K. Ariga, *Adv. Mater.*, 2012, **24**, 150–151.
11 M. Ramanathan, L. K. Shrestha, T. Mori, Q. Ji, J. P. Hill and K. Ariga, *Phys. Chem. Chem. Phys.*, 2013, **15**, 10580.
12 R. K. Iler, *J. Colloid Interface Sci.*, 1966, **21**, 569–594.
13 G. Decher and J. D. Hong, *Bunsen-Ges. Phys. Chem., Ber.*, 1991, **95**, 1430–1434.
14 G. Decher and J. D. Hong, *Makronlol. Chem., Macromol. Symp*, 1991, **46**, 321–327.
15 M. Lösche, J. Schmitt, G. Decher, W. G. Bouwman, K. Kjaer and M. Lo, *Macromolecules*, 1998, **31**, 8893–8906.
16 E. Piccinini, D. Pallarola, F. Battaglini and O. Azzaroni, *Chem. Commun.*, 2015, **51**, 14754–14757.
17 S. Y. Yang and M. F. Rubner, *J. Am. Chem. Soc.*, 2002, **124**, 2101–2102.
18 S. Takahashi, K. Sato and J. I. Anzai, *Anal. Bioanal. Chem.*, 2012, **402**, 1749–1758.
19 K. Ariga, J. P. Hill and Q. Ji, *Phys. Chem. Chem. Phys.*, 2007, **9**, 2319–2340.
20 G. Decher and J. B. Schlenoff, *Multilayer Thin Films: Sequential Assembly of Nanocomposite Materials*, Wiley-VCH Verlag GmbH & Co, 2nd edn, 2012.
21 E. Piccinini, C. Bliem, C. Reiner-Rozman, F. Battaglini, O. Azzaroni and W. Knoll, *Biosens. Bioelectron.*, 2017, **92**, 661–667.
22 D. Korneev, Y. Lvov, G. Decher, J. Schmitt and S. Yaradaikin, *Phys. B*, 1995, **213–214**, 954–956.
23 G. J. Kellogg, A. M. Mayes, W. B. Stockton, M. Ferreira, M. F. Rubner and S. K. Satija, *Langmuir*, 1996, **12**, 5109–5113.
24 D. Yoo, S. S. Shiratori and M. F. Rubner, *Macromolecules*, 1998, **31**, 4309–4318.
25 X. Arys, P. Fischer, A. M. Jonas, M. M. Koetse, A. Laschewsky, R. Legras and E. Wischerhoff, *J. Am. Chem. Soc.*, 2003, **125**, 1859–1865.
26 G. Decher, *Science*, 1997, **277**, 1232–1237.
27 D. Pallarola, N. Queralto, W. Knoll and O. Azzaroni, *Chem. – Eur. J.*, 2010, **16**, 13970–13975.
28 X. Arys, A. Laschewsky and A. M. Jonas, *Macromolecules*, 2001, **34**, 3318–3330.
29 P. Gómez-Romero and C. Sanchez, *Functional Hybrid Materials*, Wiley-VCH Verlag GmbH & Co KGaA, Weinheim, 2004.
30 T. Witten and P. Picus, *Structured Fluids: Polymers, Colloids, Surfactans*, Oxford University Press, Oxford, 2004.
31 J. A. Bouwstra, G. S. Gooris, J. A. van der Spek and W. Bras, *J. Invest. Dermatol.*, 1991, **97**, 1005–1012.
32 C. T. Kresge, M. E. Leonowicz, W. J. Roth, J. C. Vartuli and J. S. Beck, *Nature*, 1992, **359**, 710–712.
33 C. J. Brinker, Y. Lu, A. Sellinger and H. Fan, *Adv. Mater.*, 1999, **11**, 579–585.
34 C. F. J. Faul, *Acc. Chem. Res.*, 2014, **47**, 3428–3438.
35 R. Ahmed, S. K. Patra, L. Chabanne, C. F. J. Faul and I. Manners, *Macromolecules*, 2011, **44**, 9324–9334.
36 M. Antonietti, C. Burger and J. Effing, *Adv. Mater.*, 1995, **7**, 751–753.
37 M. S. Johal and P. A. Chiarelli, *Soft Matter*, 2007, **3**, 34–46.
38 M. L. Cortez, A. L. Cukierman and F. Battaglini, *Electrochem. Commun.*, 2009, **11**, 990–993.
39 M. S. Johal, B. H. Ozer, J. L. Casson, A. S. John, J. M. Robinson and H. Wang, *Langmuir*, 2004, **20**, 2792–2796.
40 X. Huang and N. S. Zacharia, *Soft Matter*, 2013, **9**, 7735–7742.
41 N. G. Caculitan, P. H. Scudder, A. Rodriguez, J. L. Casson, H. L. Wang, J. M. Robinson and M. S. Johal, *Langmuir*, 2004, **20**, 8735–8739.
42 R. J. El-Khouri and M. S. Johal, *Langmuir*, 2003, **19**, 4880–4883.
43 J. Choi and M. F. Rubner, *Macromolecules*, 2005, **38**, 116–124.
44 H. Okuda, T. Imae and S. Ikeda, *Colloids Surf.*, 1987, **27**, 187–200.
45 L. D. Sappia, E. Piccinini, W. Marmisollé, N. Santilli, E. Maza, S. Moya, F. Battaglini, R. E. Madrid and O. Azzaroni, *Adv. Mater. Interfaces*, 2017, **4**, 1700502.
46 G. Sauerbrey, *Z. Phys.*, 1959, **155**, 206–222.
47 K. A. Marx, *Biomacromolecules*, 2003, **4**, 1099–1120.
48 Z. Di, D. Posselt, D. M. Smilgies, R. Li, M. Rauscher, I. I. Potemkin and C. M. Papadakis, *Macromolecules*, 2012, **45**, 5185–5195.
49 D. Babonneau, *J. Appl. Crystallogr.*, 2010, **43**, 929–936.
50 The terms ''wet'' film refers to the mass detected by the quartz crystal microbalance (QCM) during the *in situ* assembly of successive layers. This measurement includes the mass of solvent viscoelastically coupled to the film. On the other hand, the term ''dry'' film corresponds to the mass detected by the QCM after removing the QCM sensor from the assembly solution and drying the film under a stream of N_2 gas. This experimental protocol has been popularized by Kunitake and co-workers (*J. Am. Chem. Soc.*, 1995, **117**, 6117–6123).
51 P. Kujawa, P. Moraille, J. Sanchez, A. Badia and F. M. Winnik, *J. Am. Chem. Soc.*, 2005, **127**, 9224–9234.
52 J. B. Schlenoff, H. Ly and M. Li, *J. Am. Chem. Soc.*, 1998, **120**, 7626–7634.

53 E. Piccinini, S. Alberti, G. S. Longo, T. Berninger, J. Breu, J. Dostalek, O. Azzaroni and W. Knoll, *J. Phys. Chem. C*, 2018, DOI: 10.1021/acs.jpcc.7b11128.
54 V. V. Tsukruk and S. Singamaneni, *Scanning Probe Microscopy of Soft Matter: Fundamentals and Practices*, Wiley-VCH, Weinheim, 1st edn, 2012.
55 M. Ghosh, F. Fan and K. J. Stebe, *Langmuir*, 2007, **23**, 2180–2183.
56 J. Irigoyen, S. E. Moya, J. J. Iturri, I. Llarena, O. Azzaroni and E. Donath, *Langmuir*, 2009, **25**, 3374–3380.
57 C. M. Dvoracek, G. Sukhonosova, M. J. Benedikt and J. C. Grunlan, *Langmuir*, 2009, **25**, 10322–10328.
58 M. Antonietti, J. Conrad and A. F. Thuenemann, *Macromolecules*, 1994, **27**, 6007–6011.
59 M. Antonietti and J. Conrad, *Angew. Chem., Int. Ed.*, 1994, **33**, 1869–1870.
60 G. Renaud, R. Lazzari and F. Leroy, *Surf. Sci. Rep.*, 2009, **64**, 255–380.
61 P. Busch, D. Posselt, D. M. Smilgies, M. Rauscher and C. M. Papadakis, *Macromolecules*, 2007, **40**, 630–640.
62 M. A. Modestino, D. K. Paul, S. Dishari, S. A. Petrina, F. I. Allen, M. A. Hickner, K. Karan, R. A. Segalman and A. Z. Weber, *Macromolecules*, 2013, **46**, 867–873.
63 M. A. Modestino, A. Kusoglu, A. Hexemer, A. Z. Weber and R. A. Segalman, *Macromolecules*, 2012, **45**, 4681–4688.
64 F. Marlow, I. Leike, C. Weidenthaler, C. W. Lehmann and U. Wilczok, *Adv. Mater.*, 2001, **13**, 307–310.
65 B. Platschek, N. Petkov and T. Bein, *Angew. Chem., Int. Ed.*, 2006, **45**, 1134–1138.
66 B. Platschek, R. Köhn, M. Döblinger and T. Bein, *Langmuir*, 2008, **24**, 5018–5023.
67 B. D. Vogt, C. L. Soles, H.-J. Lee, E. K. Lin and W.-L. Wu, *Langmuir*, 2004, **20**, 1453–1458.
68 J. J. Senkevich, *J. Vac. Sci. Technol., A*, 2000, **18**, 2586–2590.
69 J. L. Lenhart and W. Wu, *Macromolecules*, 2002, **35**, 5145–5152.
70 C. L. Soles, E. K. Lin, J. L. Lenhart, R. L. Jones, W. L. Wu, D. L. Goldfarb and M. Angelopoulos, *J. Vac. Sci. Technol., B*, 2001, **19**, 2690–2693.
71 K. C. Tseng, N. J. Turro and C. J. Durning, *Phys. Rev. E: Stat. Phys., Plasmas, Fluids, Relat. Interdiscip. Top.*, 2000, **61**, 1800–1811.
72 J. A. Forrest, K. DalnokiVeress and J. R. Dutcher, *Phys. Rev. E: Stat. Phys., Plasmas, Fluids, Relat. Interdiscip. Top.*, 1997, **56**, 5705–5716.
73 According to these results the adsorption of ''distorted'' micelles cannot be excluded. Indeed, we suggest that micelles can undergo a significant reorganization leading to the formation of the mesostructures.
74 A. Svensson, J. Norrman and L. Piculell, *J. Phys. Chem. B*, 2006, **110**, 10332–10340.
75 C. Gustavsson, M. Obiols-Rabasa and L. Piculell, *Langmuir*, 2015, **31**, 6487–6496.
76 C. Gustavsson, J. Li, K. J. Edler and L. Piculell, *Langmuir*, 2014, **30**, 12525–12531.
77 J.-Y. Wang, W. Chen, J. D. Sievert and T. P. Russell, *Langmuir*, 2008, **24**, 3545–3550.
78 S. Choi, E. Kim, H. Ahn, S. Naidu, Y. Lee, D. Y. Ryu, C. J. Hawker and T. P. Russell, *Soft Matter*, 2012, **8**, 3463–3469.
79 B. M. D. O'Driscoll, E. Milsom, C. Fernandez-Martin, L. White, S. J. Roser and K. J. Edler, *Macromolecules*, 2005, **38**, 8785–8794.
80 K. J. Edler and B. Yang, *Chem. Soc. Rev.*, 2013, **42**, 3765–3776.

